System-Level Modeling and Analysis of Thermal Effects in Optical Networks-on-Chip

Yaoyao Ye, *Student Member, IEEE*, Jiang Xu, *Member, IEEE*, Xiaowen Wu, *Student Member, IEEE*, Wei Zhang, *Member, IEEE*, Xuan Wang, *Student Member, IEEE*, Mahdi Nikdast, *Student Member, IEEE*, Zhehui Wang, *Student Member, IEEE*, and Weichen Liu, *Member, IEEE*

***Abstract*—The performance of multiprocessor systems, such as chip multiprocessors (CMPs), is determined not only by individual processor performance, but also by how efficiently the processors collaborate with one another. It is the communication architecture that determines the collaboration efficiency on the hardware side. Optical networks-on-chip (ONoCs) are emerging communication architectures that can potentially offer ultra-high communication bandwidth and low latency to multiprocessor systems. Thermal sensitivity is an intrinsic characteristic of photonic devices used by ONoCs as well as a potential issue. This paper systematically modeled and quantitatively analyzed the thermal effects in ONoCs. We used an 8 × 8 mesh-based ONoC as a case study and evaluated the impacts of thermal effects in the average power efficiency for real MPSoC applications. We revealed three important factors regarding ONoC power efficiency under temperature variations, and proposed several techniques to reduce the temperature sensitivity of ONoCs. These techniques include the optimal initial setting of microresonator resonant wavelength, increasing the 3-dB bandwidth of optical switching elements by parallel coupling multiple microresonators, and the use of passive-routing optical router Crux to minimize the number of switching stages in mesh-based ONoCs. We gave a mathematical analysis of periodically parallel coupling of multiple microresonators and show that the 3-dB bandwidth of optical switching elements can be widened nearly linearly with the ring number. Evaluation results for different real MPSoC applications show that, on the basis of thermal tuning, the optimal device setting improves the average power efficiency by 54% to 1.2 pJ/bit when chip temperature reaches 85 °C. The findings in this paper can help support the further development of this emerging technology.**

***Index Terms*—Multiprocessor, optical interconnect, optical network-on-chip, temperature sensitivity, thermal effect.**

I. Introduction

With the burgeoning complexity of multiprocessor systems, such as chip multiprocessors (CMPs), tens and even hundreds of processor cores are required to be integrated on a single chip. The performance of multiprocessor systems is determined not only by the performance of their processors, but also by how efficiently they collaborate with one another. It is the communication architectures that determine the collaboration efficiency on the hardware side. An efficient on-chip communication architecture can help fully utilize the computation resources offered by multiple processor cores on a CMP. On-chip communication architectures have gradually moved to network-on-chip (NoC) to alleviate the problems of poor scalability, limited bandwidth, and high power consumption in traditional interconnection networks [1], [2].

As semiconductor technologies continually shrink feature sizes and new applications demand even more on-chip communications, conventional metallic interconnects are becoming the bottleneck of NoCs. As an emerging communication architecture for new-generation multiprocessor systems, optical networks-on-chip (ONoCs) are based on photonic technologies, and can potentially offer ultra-high communication bandwidth, low latency, and high energy efficiency. Recent developments in nanoscale silicon photonic devices substantially improve the feasibility of ONoCs [3]. However, as an intrinsic characteristic of photonic devices, thermal sensitivity is a potential issue in ONoC designs. Chip temperature fluctuates temporally as well as spatially, and the steady-state temperature can vary by more than 30 °C across a chip under typical operating conditions [4]. As a result of thermo-optic effect, on-chip temperature variations can affect the characteristics of photonic devices. Such thermal effects can potentially cause ONoC performance degradation and even functional failure under large chip temperature fluctuations. An ONoC thermal model is required to fully understand these challenges and help further develop this emerging technology.

This work presented a system-level analytical thermal model for general ONoCs based on our earlier work [5], and quantitatively studied the impacts of thermal effects in an 8 × 8 mesh-based ONoC under real MPSoC applications. Our analysis shows that on-chip temperature fluctuations can dramatically reduce the worst-case power efficiency of ONoCs especially those have a large number of switching stages. Based on the ONoC thermal model, we revealed three important factors regarding ONoC power efficiency under temperature variations, including the initial setting of photonic devices, the number of switching stages in the ONoC architecture, and the bandwidth of optical switching elements. Several techniques were proposed to reduce the temperature sensitivity of ONoCs, including the optimal setting of microresonator resonant wavelength, increasing the 3-dB bandwidth of microresonators by

Manuscript received June 20, 2011; revised October 17, 2011; accepted January 04, 2012. Date of publication February 06, 2012; date of current version January 17, 2013. This work was supported in part by DAG11EG05S and RGC of the Hong Kong SAR, China.

Y. Ye, J. Xu, X. Wu, X. Wang, M. Nikdast, Z. Wang, W. Liu are with the Department of Electronic and Computer Engineering, The Hong Kong University of Science and Technology, 999077 Hong Kong (e-mail: yeyaoyao@ust.hk; jiang.xu@ust.hk; wxxaf@ust.hk; eexwang@ust.hk; mnikdast@ust.hk; zhehui@ust.hk; weichen@ust.hk).

W. Zhang is with the School of Computer Engineering, Nanyang Technological University, Singapore 639798 (e-mail: zhangwei@ntu.edu.sg).

Color versions of one or more of the figures in this paper are available online at http://ieeexplore.ieee.org.

Digital Object Identifier 10.1109/TVLSI.2012.2185524

parallel coupling multiple rings, and the use of passive-routing optical router Crux to minimize the number of switching stages in mesh-based ONoCs. Other related low-temperature-dependence techniques such as thermal tuning and microresonators with low temperature-dependent wavelength shift are also considered in our analysis. To better study ONoC characteristics, a NoC traffic benchmark suit based on realistic MPSoC applications is used for network simulation, including SPEC fpppp, H.264 decoder with high resolution, sample rate converter, and satellite receiver. For each application, an offline optimization approach is applied for task mapping and scheduling onto an 8 $\times$ 8 optical mesh NoC-based MPSoC. We evaluated the average power efficiency under different combinations of device setting and low-temperature-dependence techniques. Evaluation results show that by properly setting the initial device conditions, the power efficiency is improved by 54% to 1.2 pJ/bit (under 30 °C spatial temperature variation) on average of the four MPSoC applications.

The rest of paper is organized as follows. Section II gives a survey of related works on ONoCs and the investigations of thermal sensitivity in photonic devices. Section III proposes the ONoC thermal model based on detailed analysis of thermal effects in each individual component of a general ONoC. Section IV presents different techniques to reduce the temperature sensitivity of ONoCs. In Section V, we use a mesh-based ONoC as a case study and quantitatively analyze the temperature-dependent average power efficiency under different real MPSoC applications. Section VI draws the conclusions of this work.

II. Related Works

With the booming developments in nanoscale silicon photonic technologies for short-haul communication, different ONoC architectures have been developed based on optical waveguides and microresonators. Kirman *et al.* proposed a hierarchical optical bus for multiprocessor systems [6]. Briere *et al.* presented a multistage ONoC with a passive-switching *λ—router* [7]. Beausoleil *et al.* proposed a crossbar-based ONoC [8]. Shacham *et al.* proposed an augmented-torus ONoC based on 4 $\times$ 4 optical switches [9]. Mo *et al.* proposed a hierarchical mesh-based ONoC [10]. Pasricha *et al.* presented an ONoC based on an optical ring with bus protocol standards [11]. Pan *et al.* proposed an optical crossbar with localized arbitration [12]. Gu *et al.* proposed a fat-tree based ONoC [13]. Cianchetti *et al.* proposed an optical network based on low-latency predecoded source routing [14]. Kodi *et al.* proposed an ONoC architecture with static routing and wavelength allocation [15]. Ding *et al.* presented an optical routing framework to reduce the power consumption of ONoCs [16]. The total cost of on-chip optical modulator is formulated and minimized with the technique of integer linear programming under various detection constraints. Batten *et al.* proposed an optical mesh based on a hybrid optical-electrical global crossbar, where processing cores and DRAM are divided into sub-mesh and connected with the optical crossbar [17].

Though ONoCs offer a new approach to empowering ultra-high bandwidth with low power consumption, there are also voices of concern about the reliability of optical interconnection for on-chip applications. An investigation of thermal issues of on-chip optical interconnects shows that, with the consideration of thermal regulation power, optical interconnects may not have advantages in power efficiency as compared with their electrical counterpart [18]. Another work analyzed the reliability challenges in nanophotonic on-chip networks and proposed a run-time reliability management solution [19]. The proposed hardware-software management technique uses device-level voltage tuning to compensate intra-core fabrication-induced process variation and intra-core temperature variation. For inter-core variations, system-wide work migration is combined with dynamic voltage and frequency scaling (DVFS) for temperature control and performance optimization.

More device-level investigations of thermo-optic effect have been carried out in literature. As a result of thermo-optic effect, material refractive index changes with temperature. For example, the thermo-optic coefficient (dn/dT) of silicon is on the order of 10^{-4}/K. This will cause changes in silicon-based photonic device characteristics under temperature variations. The temperature-dependent wavelength shift in silicon-based microresonators is found to be about 50–100 pm/K, which is non-negligible in practical use [20]–[22]. As a widely used device in ONoCs, microresonator performs as a wavelength-selective optical switch or modulator. The undesired wavelength mismatch caused by temperature variation will result in additional optical power loss. Thermal tuning by local microheaters is an alternative solution to compensate the temperature-dependent wavelength shift for microresonators. And the tuning efficiency in current technology is on the order of several mW/nm [23], [24]. Besides thermal tuning, there are also researches of passive compensation techniques for microresonators. Microresonators with low temperature dependence or even athermal microresonators have been demonstrated in literature [25], [26]. The main idea of these techniques is to apply proper polymer materials (with negative thermo-optic coefficient) as upper cladding of silicon microresonators, or using slot waveguide structure.

Other optical link modules such as laser source and optical receiver are also sensitive to temperature variations. Investigations of the temperature sensitivity of vertical cavity surface emitting laser (VCSELs) show that the temperature-dependent wavelength shift is comparable to or even larger than that of microresonators [27], [28]. Further more, because of the mutual shift between lasing wavelength and peak material gain wavelength under temperature variations, VCSEL power efficiency degrades seriously at high temperatures [29]. There are also investigations of the temperature-dependent behaviors of Ge-based photodetectors [30], [31]. Temperature sensitivity of the whole ONoC should be considered during ONoC architecture design and power efficiency evaluation. In this work, an ONoC thermal model was developed based on the analysis of thermal sensitivity for every optical link module, and several techniques were proposed to reduce the temperature sensitivity of ONoCs. We used an 8 $\times$ 8 mesh-based ONoC as a case study and evaluated the thermal effects in the average power efficiency for real MPSoC applications.

III. ONoC Thermal Model

ONoCs rely on optical signals to communicate payload data as well as control information among processor cores and

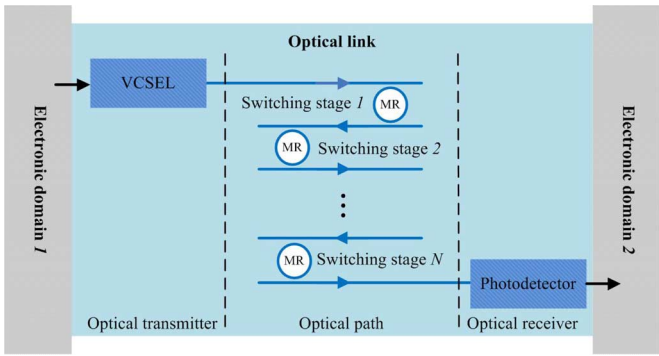

Fig. 1. Overview of the optical link in ONoCs connecting two electronic domains.

memories. In different ONoC architectures, optical signals are transmitted through different optical links between sources and destinations. Most ONoC architectures employ photonic devices which can be integrated with existing CMOS-based processor cores either through CMOS-compatible fabrication processes or bonding technologies. Despite the architecture diversity, an optical link in ONoCs is generally composed of an optical transmitter, an optical path, and an optical receiver (see Fig. 1). The optical transmitter can convert electrical signals into optical signals by directly modulating the driving current of a VCSEL [29] or using an optical modulator. In this work, we assume to use VCSELs as the laser source for ONoCs and use 3-D integration technology to connect VCSELs with the underlying CMOS driver circuits through TSVs (through silicon via). The output power of VCSELs is directly modulated by the driving current. The optical receiver uses photodetectors to convert optical signals into electrical signals used by processors or memories in electronic domains. A typical receiver also includes transimpedance amplifier (TIA) and limiting amplifier (LA) circuits for current-to-voltage conversion and voltage amplification. On the optical path between the transmitter and receiver, multiple switching elements switch optical signals in stages onto a series of optical waveguides until reaching the destination. Microresonator-based add-drop filters have been widely used as the switching element to perform the switching function in ONoCs [9], [12], [13]. In this work, we focus on how temperature variations affect the characteristics of photonic devices in ONoCs. We systematically analyzed the relationship between different components and presented related characteristics from a system-level point of view, which also served as the necessary basis for our ONoC thermal model.

A. On-Chip Temperature Variation and Thermo-Optic Effect

The absolute temperature and temperature fluctuations across the chip die have been major concerns in chip design and packaging because a high temperature could cause performance degradation and even functional failures in CMOS circuits. Transient thermal analysis shows that chip temperature responds power changes quickly at the beginning and takes a relatively long time to reach the steady state [32]. Steady-state chip temperature also varies spatially because of the nonuniform power densities across the chip as well as the limited thermal conductivity of the die and packaging materials. For example, in Intel Itanium processor which is under stringent thermal management, while some part of the chip can be maintained at a relatively low temperature of 60 °C, the other part of chip can still reach about 88 °C [33]. In general, the maximum junction temperature on chip is 25 °C higher than the average [34], and chip temperatures can vary by more than 30 °C across the chip under typical operating conditions [4].

As a result of thermo-optic effect, material refractive index is temperature dependent and follows (1), where n_0 is the refractive index at room temperature, dn/dT is the thermo-optic coefficient of the material, and ΔT is the temperature variation

$$n = n_0 + \frac{dn}{dT}\Delta T. \tag{1}$$

Physical measurements show that the thermo-optic coefficient of silicon is on the order of 10^{-4}/K and is nonlinear over a large temperature range at 1550 nm wavelength [35]. Within the chip temperature range, the second-order polynomial interpolation of the measurement results follows (2), where the temperature T is in Kelvin

$$\frac{dn_{Si}}{dT} = 8.61 \times 10^{-5} + 3.63 \times 10^{-7} \times T - 2.07 \times 10^{-10} \times T^2. \tag{2}$$

Since refractive index is an important device parameter, the thermo-optic effect will cause changes in device characteristics. For microresonator, the resonance wavelength is directly governed by the effective refractive index, and the resonance wavelength red-shifts with increasing temperatures. For VCSELs, the emission wavelength will also shift with changing temperatures. In the following sessions, we will systematically analyze the thermal sensitivity for each optical component in a general on-chip optical interconnect and develop a thermal model for ONoCs.

B. Thermal Sensitivity of Optical Transmitters

Optical transmitters convert electrical signals into optical signals by either directly modulating the driving current of VCSELs, or using an optical modulator. Optical modulators can be used to indirectly modulate the optical signal outputted by VCSELs or off-chip laser sources. VCSELs are a good candidate for on-chip laser source because of the low power consumption, high modulation bandwidth and manufacturing advantages. For 1550-nm VCSELs, data rates beyond 10 Gbps have been demonstrated [29]. The single-mode output of VCSEL is on the order of several mW. As demonstrated in [36], VCSELs can be bonded to CMOS integrated circuits. Assume that every VCSEL is of 55 μm diameter, 64 VCSELs need a total area of 0.2 mm^2. Based on the rapid technology advancements in recent years, VCSELs provide an opportunity for better integration and are chosen by many ONoC architectures to fully integrate ONoCs on CMPs. The characteristics of VCSELs are sensitive to temperature changes. As for off-chip lasers equipped with temperature control units, the laser can be set at a fixed wavelength but it consumes extra power. In this work, since we focus on thermal aspects, we assume VCSELs as the laser source and consider their thermal variations when developing the ONoC thermal model.

As in (3), the emission wavelength λ_{VCSEL} is determined by the cavity resonance, where n_{ave} is the spatially averaged refractive index of the laser cavity, l_{VCSEL} is the cavity length, and m_{VCSEL} is the resonance order [27]. The temperature-dependent wavelength shift of VCSEL emission is mainly governed by the change of n_{ave} under temperature variations

$$l_{\mathrm{VCSEL}} \cdot n_{\mathrm{ave}} = m_{\mathrm{VCSEL}} \cdot \lambda_{\mathrm{VCSEL}}/2. \tag{3}$$

For VCSELs in the emission wavelength range 800–1000 nm, the temperature-dependent wavelength shift of the cavity resonance is typically found to be 0.07 nm/°C, and the shift of the peak material gain wavelength is about 0.32 nm/°C [27]. The investigation of a 1300 nm VCSEL shows a similar result [28].

Besides the temperature-dependent wavelength shift, the power efficiency of VCSELs degrades with increasing temperature as a result of thermal effects on the threshold current and slope efficiency. Because of the different temperature-dependent shift of cavity resonance and peak gain, a mutual shift between the lasing mode and gain spectrum occurs when temperature changes. The misalignment causes the threshold current I_{th} of VCSEL to increase with temperature T following an approximate parabolic shaped curve shown by (4), where α is the minimum threshold current, β is a coefficient related to the gain properties, and T_{th} is the temperature at which the cavity resonance is spectrally aligned with the peak gain [37]

$$I_{th} = \alpha + \beta(T - T_{th})^2. \tag{4}$$

If the driving current is above the threshold, the output power will increase approximately linearly with the driving current. Slope efficiency is the incremental increase in output power for an incremental increase in driving current. The slope efficiency decreases approximately linearly with an increasing temperature, and can be expressed by (5), where ε is the slope efficiency at 0 °C, and γ is a positive coefficient

$$s = \varepsilon - \gamma \cdot T. \tag{5}$$

For the VCSEL demonstrated in [29], when the temperature changes from room temperature to 80 °C, the slope efficiency decreases from 0.36 to 0.23 mW/mA, and the maximum emission power decreases from 4 to 1.5 mW correspondingly. We take the degradation of VCSEL power efficiency into account when developing the ONoC thermal model, based on the LIV characteristics of VCSELs demonstrated in [29].

C. Thermal Sensitivity of Switching Elements

On the optical path between the transmitter and receiver, multiple switching elements switch optical signals in stages onto a series of optical waveguides until reaching their destination. Microresonators of different structures have been widely used as the switching elements to perform the switching function in ONoCs. The switching functionality a ring-based microresonator can be illustrated by a simplified model shown in Fig. 2.

In the simplified model, a microresonator has two distinctive states, on state and off state. In the on state, the resonant wavelength of the microresonator is the same as the wavelength of input optical signals, and the optical signals will be coupled to the drop port. In the off state, the microresonator shifts to a different resonant wavelength from the one carried the input optical signals, and the optical signals will propagate directly to the through port. ONoCs set the resonant wavelength of microresonators according to network routing information to establish optical paths between transmitters and receivers. The peak resonant wavelength λ_{MR} of a microresonator obeys the relationship in (6), where l_{MR} is the one-round length of the ring, m_{MR} is an integer indicating the order of the resonance, and n_{eff} is the effective index of the waveguide mode involved in the resonance

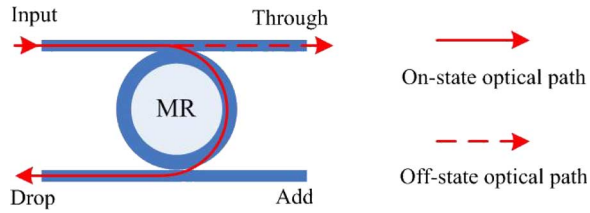

Fig. 2. Simplified model for the switching functionality of a ring-based microresonator.

$$l_{\mathrm{MR}} \cdot n_{\mathrm{eff}} = m_{\mathrm{MR}} \cdot \lambda_{\mathrm{MR}}. \tag{6}$$

With a constant l_{MR} and m_{MR}, the peak resonant wavelength λ_{MR} will change in proportion with n_{eff}. Since n_{eff} changes with the temperature, the peak resonant wavelength will also vary with the temperature. Both theoretical analysis and experiment results confirm a linear relationship between the resonant wavelength shift and temperature. The linear relationship can be expressed as (7), where ρ_{MR} is defined as the microresonator temperature-dependent wavelength shift coefficient, $\lambda_{\mathrm{MR\_0}}$ is the resonant wavelength at the initial temperature, σ_{eff} is the thermo-optic coefficient (dn/dT) of the effective index, and n_g is the group index of the waveguide [38]

$$\rho_{\mathrm{MR}} = \frac{\lambda_{\mathrm{MR\_0}}}{n_g} \cdot \sigma_{\mathrm{eff}}. \tag{7}$$

For a 500×220 nm^2 Si/SiO_2 waveguide, the group index is about 4.2 [22] and the effective index changes slower than the refractive index of silicon ($(dn_{Si}/dT) \approx 1.86 \times 10^{-4}$/°C). Based on (7), silicon microresonators red-shift the resonant wavelength about 58 pm per °C. Experiments show a similar result where the temperature-dependent wavelength shift of microresonator is found to be 50 pm per °C [20].

An ideal lossless microresonator would confine light indefinitely, but intrinsic loss always exists in any physical implementation of cavities. The deviation from the ideal condition is defined by the quality factor Q, which is proportional to the confinement time of the cavity. The total quality factor of a ring-based microresonator used in Fig. 1 is defined by (8), where λ_{MR} is the resonant wavelength, 2δ is the 3-dB bandwidth of the drop-port power transfer spectrum, κ_e^2 is the fraction of power coupling between the input waveguide and the ring, κ_d^2 is the fraction of power coupling between the drop waveguide and the

ring, and κ_p^2 is the power loss per round-trip of the ring [39]. Microresonators with Q ranging from 1500 to 100 000 have been demonstrated using different structures [40]

$$Q = \frac{\lambda_{\mathrm{MR}}}{2\delta} = \frac{2\pi n_g l_{\mathrm{MR}}}{\lambda_{\mathrm{MR}}\left(\kappa_e^2 + \kappa_d^2 + \kappa_p^2\right)}. \tag{8}$$

Microresonators have a Lorentzian power transfer function which is peaked at the resonant wavelength λ_{MR}. For optical signals carried on wavelength λ_s, the drop-port power transfer can be expressed as (9) [41]. When $\kappa_d^2 + \kappa_e^2 \gg \kappa_p^2$, nearly full power transfer can be achieved at the peak resonance point, and the microresonator will exhibit a low insertion loss. Physical implementations show that the insertion loss of a microresonator can be practically lowered to 0.5 dB [42]

$$\frac{P_{\mathrm{drop}}}{P_{\mathrm{in}}} = \left(\frac{2\kappa_e\kappa_d}{\kappa_e^2 + \kappa_d^2 + \kappa_p^2}\right)^2 \cdot \frac{\delta^2}{(\lambda_s - \lambda_{\mathrm{MR}})^2 + \delta^2}. \tag{9}$$

According to (9), a deviation from the peak resonant wavelength would result in more power loss at the drop port especially for a high-Q microresonator. For a microresonator at the 1550 nm wavelength range, if the quality factor Q is on the order of 10^4, a 10 °C temperature change would make the power spectrum shift about 0.5 nm and result in a power loss variation of about 16 dB for optical signals carried by 1550 nm wavelength. The loss variation would increase to 22 dB for a 20 °C temperature change and 26 dB for a 30 °C temperature change. For ONoCs requiring multiple switching stages on each optical link, the problem can become even more serious as multiple switching elements could reduce the optical signal strength significantly (see Fig. 1).

D. Thermal Sensitivity of Optical Waveguides

ONoCs use optical waveguides to connect transmitters, switching elements, and receivers together to form optical links. Silicon-based waveguides can be fabricated on silicon-on-isolator (SOI) substrate with a silicon slab on top of a buried oxide (BOX) layer which prevents optical mode from leaking to the substrate. The cross-section of a single-mode waveguide can be designed to be 510 nm × 226 nm with minimum propagation loss and group velocity dispersion [43]. As a result of the thermo-opti effect, both the waveguide propagation loss and latency are temperature dependent.

1) Propagation Loss Variation in Optical Waveguide: The silicon core of a waveguide has negligible absorption of energy and the propagation loss is dominated by the sidewall roughness scattering. Propagation loss in a straight optical waveguide can be estimated by (10), where ϵ is a parameter regarding the interface roughness, k_0 is the free space wavenumber, β is the modal propagation constant, h is the transverse propagation constant in the waveguide core, ϕ is the refractive index difference between the waveguide core and cladding materials, and $E_s^2/\int E^2 dx$ is the normalized electric field intensity at the waveguide core/cladding interface [44]

$$L_{\mathrm{WG}} = \frac{4\epsilon^2 k_0^2 h}{\beta} \cdot \frac{E_s^2}{\int E^2 dx} \cdot \phi^2. \tag{10}$$

As shown in (10), the waveguide propagation loss is proportional to the refractive index difference between the core and cladding. Because of the different thermo-optic coefficients (dn/dT) of the core and cladding materials, the propagation loss will also change with operating temperatures. Assume that the temperature along the waveguide is uniformly distributed between T_0 and $T_0 + \Delta T$, the corresponding waveguide propagation loss variation is expressed in (11), where $L_{\mathrm{WG\_0}}$ is the propagation loss at room temperature T_0. σ_c and σ_d are defined as the thermo-optic coefficients (dn/dT) of the waveguide core and cladding materials, respectively. For an optical waveguide with a Si core and SiO_2 cladding, the refractive index difference ϕ is approximately equal to 2

$$L_{\mathrm{WG}} = L_{\mathrm{WG\_0}} \cdot \left(1 + \frac{\sigma_c - \sigma_d}{\phi} \cdot \Delta T + \frac{(\sigma_c - \sigma_d)^2}{3\phi^2} \cdot (\Delta T)^2\right). \tag{11}$$

Based on (11), the propagation loss variation on a Si/SiO_2 waveguide is about 0.22% for $\Delta T = 30\,^{\circ}\mathrm{C}$. Waveguide propagation loss is less sensitive to temperature compared to the insertion loss of high-Q switching elements.

2) Latency Variation in Optical Waveguide: For an optical waveguide with a length of l_{WG}, the light latency D_{WG} is as (12), where c is the light speed in vacuum, and n_g is the waveguide group index

$$D_{\mathrm{WG}} = \frac{l_{\mathrm{WG}}}{c} \cdot n_g. \tag{12}$$

Because of the thermo-optic effect in n_g, the waveguide latency is also temperature dependent. High latency variation would lower the data rate. Assume that the temperature along the waveguide is not consistent, by taking the derivative of D_{WG} [see (12)] with respect to temperature T, we get the temperature-dependent variation coefficient of the waveguide latency in (13). dn_g/dT is the group thermo-optic coefficient of the waveguide

$$\frac{dD_{\mathrm{WG}}}{dT} = \frac{l_{\mathrm{WG}}}{c} \cdot \frac{dn_g}{dT}. \tag{13}$$

Assume that the temperature along the waveguide is uniformly distributed between T_0 and $T_0 + \Delta T$, the latency variation can be estimated as (14)

$$\Delta D_{\mathrm{WG}} = \frac{l_{\mathrm{WG}}}{c} \cdot \frac{dn_g}{dT} \cdot \frac{\Delta T}{2}. \tag{14}$$

For a 500×220 nm^2 Si/SiO_2 waveguide, the group index n_g of the TE mode is about 4.2 at 1550 nm wavelength [22]. For a waveguide length of $l_{\mathrm{WG}} = 10$ mm, the light latency D_{WG} is 0.14 ns if the whole waveguide is at room temperature. Assume that $(dn_g/dT) = 3.1 \times 10^{-4}$ [45], if the temperature along the waveguide is uniformly distributed between T_0 and $T_0 + 30\,^{\circ}\mathrm{C}$, the latency variation is 0.15 ps. If the temperature changes by $\Delta T = 85\,^{\circ}\mathrm{C}$, the latency variation would be about 0.425 ps. High latency variation might lower the data rate. Since

the thermal variation of waveguide latency is small, we neglect it

$$L_{\mathrm{SW}} = \sum_{i=1}^{N} 10\log\left(\left(\frac{2\kappa^2+\kappa_p^2}{2\kappa^2}\right)^2 \cdot \left(1+\left(\lambda_{\mathrm{VCSEL\_min}} + \rho_{\mathrm{VCSEL}}(T_{\mathrm{VCSEL}}-T_{\min}) - \rho_{\mathrm{MR}}(T_{\mathrm{MR_i}}-T_{\min}) - \lambda_{\mathrm{MR\_min}}\right)^2/\delta^2\right)\right). \quad (15)$$

E. Thermal Sensitivity of Optical Receivers

Optical receivers use photodetectors for optical-to-electrical conversion. Most photodetector designs use Ge as the absorbing material because of the high absorption coefficient of Ge in the near infrared spectrum as well as its compatibility with CMOS fabrication processes. The photodetector converts optical signals into electrical current and the subsequent TIA-LA circuits then convert electrical current to the logic level. By monolithically integrating Ge-based photodetector with high-speed TIA-LA circuits, a 10 Gbps optical receiver can achieve a sensitivity of -14.2 dBm with a bit error rate (BER) of 10^{-12} in the 1550 nm wavelength range [46]. Another work reported a better receiver sensitivity of -18.9 dBm for the same BER at a lower data rate of 5 Gbps [47].

A major concern for the temperature-dependent behaviors of Ge-based photodetectors is the potential excessive dark current under high operating temperatures. Studies show that the dark current of a 10 μm $\times$ 10 μm Ge-on-SOI photodetector increases from 20 to 192 nA when temperature change from room temperature to 86 °C, while the receiver sensitivity does not have obvious change [30]. In high-speed optical receiver designs, 1 μA is generally regarded as the upper limit of the tolerable dark current. Although the dark current of a photodetector increases with temperature, it is still sufficiently low so as not to degrade the receiver performance even under a high operating temperature. Researches on the thermal performance of Ge-based photodetectors report similar conclusions. For example, in [31], the dark current of circular Ge photodetectors with diameters of 35–250 μm increases by a factor of nine from 30 °C to 85 °C, but the sensitivity of the optical receiver does not have obvious change. Based on above observations, we assume that the sensitivity of the optical receiver does not change with the operating temperature in our ONoC thermal model.

F. ONoC Thermal Model

To ensure that ONoCs function properly, a necessary condition is that the optical signal power received by the receiver of an optical link should not be lower than the receiver sensitivity. We assume that the sensitivity is -14.2 dBm for a BER of 10^{-12} [46]. This condition must hold, otherwise the BER would increase. We model the condition in (16), where P_{TX} is the output power of the optical transmitter on a link, L_{SW} is the optical power loss due to the switching elements, L_{WG} is the optical power loss due to the waveguides, and S_{RX} is the sensitivity of the receiver

$$P_{\mathrm{TX}} - L_{\mathrm{SW}} - L_{\mathrm{WG}} \geq S_{\mathrm{RX}}. \quad (16)$$

As analyzed earlier, the output power of VCSELs degrades at higher operating temperatures. Assuming that the VCSEL is driven by current I which is above the threshold but before the point where the output power starts to decrease with current, we can express P_{TX} by (17), where $T_{\mathrm{VCSEL}} \in [T_{\min}, T_{\max}]$ is the VCSEL operating temperature, and α, β, ε, and γ are positive parameters we defined in the earlier section

$$P_{\mathrm{TX}} = \left(I - \alpha - \beta(T_{\mathrm{VCSEL}} - T_{th})^2\right)(\varepsilon - \gamma \cdot T_{\mathrm{VCSEL}}). \quad (17)$$

The spatial temperature fluctuations in ONoCs will result in mismatches between the VCSELs lasing wavelength and the resonant wavelength of switching elements. The lasing wavelength of VCSELs red-shift approximately linearly with temperature, which can be calculated by (18). $\lambda_{\mathrm{VCSEL\_min}}$ is the VCSEL lasing wavelength at temperature $T_{\min}$, and ρ_{VCSEL} is defined as the temperature-dependent wavelength shift coefficient of VCSELs

$$\lambda_{\mathrm{VCSEL}} = \lambda_{\mathrm{VCSEL\_min}} + \rho_{\mathrm{VCSEL}}(T_{\mathrm{VCSEL}} - T_{\min}). \quad (18)$$

The resonant wavelengths of microresonators also red-shift approximately linearly with increasing temperatures. For a microresonator working at temperature $T_{\mathrm{MR}} \in [T_{\min}, T_{\max}]$, the resonant point is as in (19), where $\lambda_{\mathrm{MR\_min}}$ is the resonant wavelength at $T_{\min}$ and ρ_{MR} is the temperature-dependent wavelength shift coefficient of microresonators

$$\lambda_{\mathrm{MR}} = \lambda_{\mathrm{MR\_min}} + \rho_{\mathrm{MR}}(T_{\mathrm{MR}} - T_{\min}). \quad (19)$$

Considering the thermal-induced wavelength mismatches on an optical link with N switching stages, the optical power loss due to the switching elements L_{SW} can be calculated by (15). We assume that all the switching elements in the ONoC are identical and symmetrically coupled with a ring-waveguide coupling efficiency of κ^2. κ_p^2 and δ are parameters we defined in earlier section. Microresonators in different switching stages could work at different temperatures, and we assume that the microresonator at the i_{th} switching stage works at temperature $T_{\mathrm{MR_i}}(T_{\min} \leq T_{\mathrm{MR_i}} \leq T_{\max})$.

Based on the above analysis, we can get the ONoC thermal model in (20). The last term of the equation is the optical power loss due to the waveguides on the optical link. The thermal model shows that under a high power loss in the optical path caused by chip temperature fluctuations, more input power would be needed by the transmitter to guarantee enough optical power reaching the receiver. The thermal-induced optical power received at the end of an ONoC link can be calculated by the left-hand side of (20)

$$10\log\left(\left(I - \alpha - \beta(T_{\mathrm{VCSEL}} - T_{th})^2\right)(\varepsilon - \gamma \cdot T_{\mathrm{VCSEL}})\right) - \sum_{i=1}^{N} 10\log\left(\left(\frac{2\kappa^2+\kappa_p^2}{2\kappa^2}\right)^2\right.$$

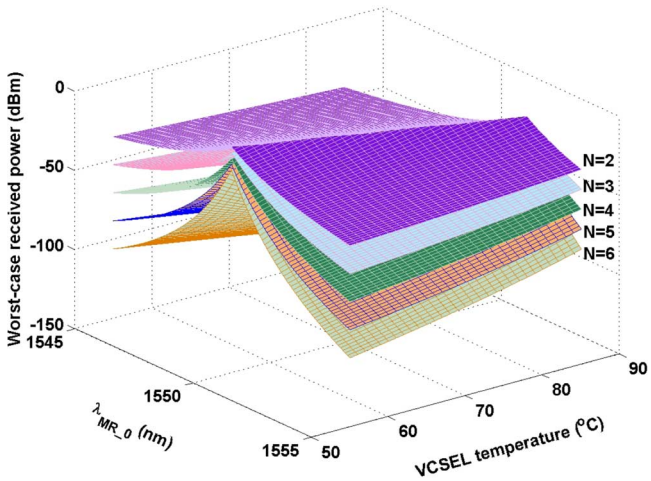

Fig. 3. Worst-case optical power received at the receiver.

$$\cdot \left(1+\delta^{-2}\left(\lambda_{\mathrm{VCSEL\_min}} + \rho_{\mathrm{VCSEL}}(T_{\mathrm{VCSEL}} - T_{\min}) - \rho_{\mathrm{MR}}(T_{\mathrm{MR_i}} - T_{\min}) - \lambda_{\mathrm{MR\_min}}\right)^2\right)\Bigg) - L_{\mathrm{WG}} \geq S_{\mathrm{RX}}. \quad (20)$$

A closer study of the thermal model reveals several thermal properties of ONoCs. First, the number of switching stages N in an optical link can dramatically change the thermal-induced power consumption. Second, initial device settings can affect the thermal-induced power consumption. Third, the 3-dB bandwidth of the switching elements is an important factor of the thermal-induced power consumption. High-Q microresonator-based switching elements have narrow passbands and will be more sensitive to the thermo-optic effects as compared with those with wider passbands. A detailed quantitative analysis of those properties is presented in Section IV.

IV. Techniques to Reduce the Temperature Sensitivity of ONoCs

Based on the analytical ONoC thermal model, we found the optimal device settings for ONoCs and analyzed different techniques to reduce the temperature sensitivity of ONoCs.

A. Optimal Initial Setting of Photonic Devices

Fig. 3 shows the worst-case optical power reaching the receiver. The worst-case analysis is conducted among all possible thermal maps where the chip temperature varying spatially between 55 °C and 85 °C. N is the number of switching stages. We assume the lasing wavelength of VCSELs is 1550 nm at 25 °C and the temperature-dependent wavelength shift ρ_{VCSEL} is 0.09 nm/°C. We assume that the driving current of VCSEL is 12 mA and the 3-dB bandwidth of microresonators is 1.55 nm. The minimum threshold current α of VCSELs is assumed to be 2.4 mA at $T_{th} = 40\,^{\circ}\mathrm{C}$, with $\beta = 0.00075$, $\varepsilon = 0.403$, and $\gamma = 0.00217$ [29]. The waveguide loss is assumed to be 4.6 dB including 3.4 dB waveguide propagation loss for a path length of 20 mm [43]. We assume the initial resonant wavelength of microresonators $\lambda_{\mathrm{MR\_0}}$ at room temperature is in the range of 1545 to 1555 nm, and the temperature-dependent wavelength shift ρ_{MR} is 0.06 nm/°C.

Fig. 3 shows that the worst-case optical power received at the destination decreases quickly as the number of switching stages increases. This indicates the importance of keeping a small number of switching stages in ONoC design. Fig. 3 also shows that the worst-case power loss under temperature variations has a upper bound, which indicates that the worst-case thermal-induced power loss can be minimized by properly setting the initial device conditions. We find that the lowest worst-case power loss can be reached by setting $\lambda_{\mathrm{MR\_0}}$ and $\lambda_{\mathrm{VCSEL\_0}}$ according to (21), where T_0 is the room temperature. The equation shows that $\lambda_{\mathrm{MR\_0}}$ should be moderately larger than $\lambda_{\mathrm{VCSEL\_0}}$ if ρ_{VCSEL} is slightly larger than ρ_{MR}

$$\lambda_{\mathrm{MR\_0}} = \lambda_{\mathrm{VCSEL\_0}} + \frac{(\rho_{\mathrm{VCSEL}} - \rho_{\mathrm{MR}})}{2} \cdot (T_{\max} + T_{\min} - 2T_0). \quad (21)$$

B. Reduce the Temperature Dependence of Microresonators

Because of the thermo-opti effect, both VCSELs and silicon-based microresonators have a temperature-dependent wavelength shift on the order of 50–100 pm/°C. Under a nonuniform temperature distribution across the chip, wavelength mismatches between the lasing wavelength of source VCSEL and the resonant wavelength of microresonators at switching stages could cause an excessive optical power loss. Thermal tuning of microresonators by local microheaters is an alternative solution to compensate the thermal-induced variation as well as the fabrication error. Tuning efficiency of several mW/nm has been demonstrated in related research works [23].

Another possible solution is to fabricate microresonators with low temperature dependence or even athermal microresonators. Related researches show that by applying proper polymer materials as upper cladding or using slot waveguide structure, the temperature-dependent wavelength shift of silicon-based microresonators can be reduced to a few pm/°C or even be totally compensated [25], [26]. After replacing temperature-sensitive microresonators with athermal microresonators, wavelength mismatch during light switching in microresonators could still exist. This is due to the instability of VCSELs lasing under temperature variations. This indicates that even with athermal microresonators, the problem of thermal-induced wavelength mismatch can not be solved directly if using on-chip VCSELs as the laser source. In order to minimize thermal effect, the optimal setting of microresonator resonance condition we got in (21) should be applied together with the technique of athermal microresonators. In this case, the microresonator temperature-dependent wavelength shift ρ_{MR} should be set to zero when finding the optimal condition.

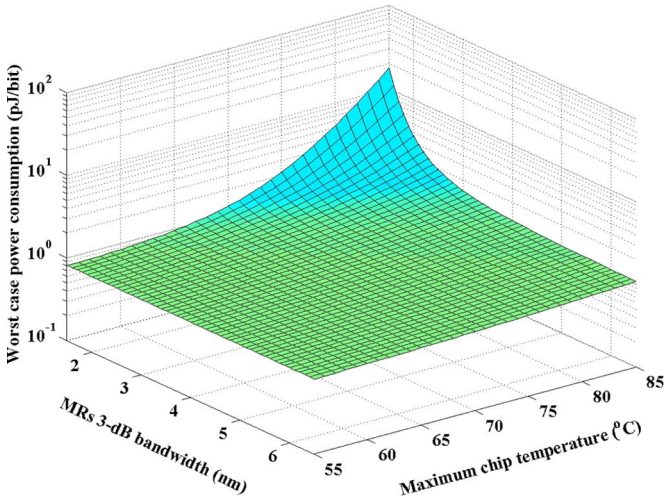

Fig. 4. Worst-case power consumption under different microresonator 3-dB bandwidths.

C. Increase the 3-dB Bandwidth of Optical Switching Elements by Parallel Coupling Microresonators

In the above sections, we already discussed several techniques including optimal device setting and microresonators with low temperature dependence. Based on the ONoC thermal model [see (20)], we find that the 3-dB bandwidth 2δ of optical switching elements is another important factor regarding temperature sensitivity. Fig. 4 shows the worst-case power consumption under different microresonator bandwidths. $\lambda_{\mathrm{MR\_0}}$ is optimal and microresonators are athermal. The number of switching stage N is three. It shows that the worst-case thermal-induced power consumption increases drastically with decreasing 3-dB bandwidth. High-Q microresonator-based switching elements with narrow 3-dB bandwidth are much more sensitive to temperature variations.

Single-ring add-drop filters (see Fig. 2) have a Lorentzian power transfer function whose 3-dB bandwidth is in inverse ratio with the total quality factor Q. High-order filters involving multiple rings were proposed to modify the drop-port spectral response, e.g., to get a more box-like spectral response with high out-of-band signal rejection ratio [48]. In a parallel-coupled high-order filter (see Fig. 5), all microresonators are directly coupled to the input and output waveguides. Signals to be dropped would pass through all the rings simultaneously, and the spacings between adjacent rings determine the drop-port power transfer. In this work, we give a mathematical analysis of the drop-port power transfer in periodical parallel-coupling with resonance deviations between neighboring microresonators, and show that the 3-dB bandwidth of the filter can be widened nearly linearly with the ring number.

In a periodically parallel-coupled filter (see Fig. 5), the overall amplitude transmission from the input port to the drop port can be found by application of the recursive formula in (22), where the recursion starts with $f_1 = r_1$ [49]. r_n and t_n^i are the amplitude transmission from the input port to the drop port and through port respectively for ring n in isolation [50]. t_n^o is the amplitude transmission from the add port to the drop port. $\theta_n = 2\pi L_n/\lambda$ is the phase delay along the waveguide between

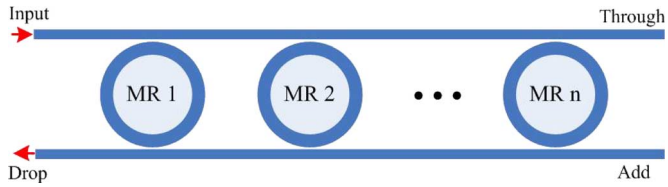

Fig. 5. Periodically parallel-coupled high-order add-drop filter.

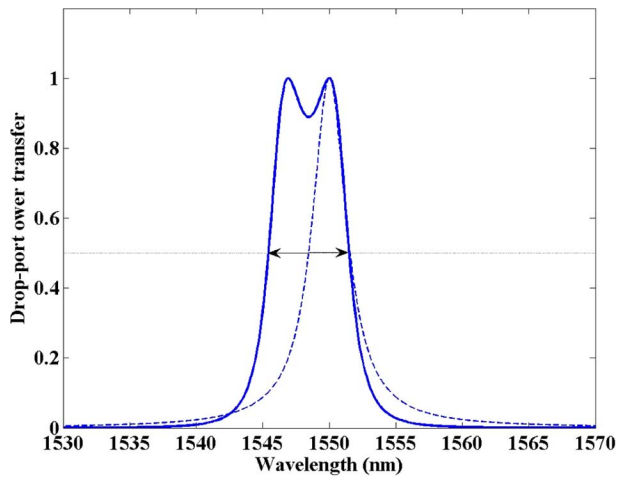

Fig. 6. Drop-port power transfer function of the two-ring parallel-coupled add-drop filter, assuming $\theta = 2\pi N + \pi/2$ and $\kappa_p^2/\kappa^2 \ll 1$.

the reference planes of ring n and ring $n+1$, where L_n is the spacing between the two rings and λ is the wavelength in free space. $\tau = 2\pi R n_g/c$ is the round-trip propagation time in microresonator. We assume that microresonators in the array are coupled to waveguides with $\kappa_e^2 = \kappa_d^2 = \kappa^2$. ω_n is the resonance frequency of ring n

$$f_n = r_n - \frac{t_n^i t_n^o}{r_n - f_{n-1}^{-1}\exp(j2\theta_{n-1})} \tag{22}$$

$$r_n = \frac{2\kappa^2}{j2\tau(\omega-\omega_n) + \left(2\kappa^2 + \kappa_p^2\right)} \tag{23}$$

$$t_n^i = t_n^o = \frac{j2\tau(\omega-\omega_n) + \kappa_p^2}{j2\tau(\omega-\omega_n) + \left(2\kappa^2 + \kappa_p^2\right)}. \tag{24}$$

To get a spectral response with wider 3-dB bandwidth, microresonators in parallel coupling could have some misalignment in resonance frequency. For a two-ring parallel-coupled add-drop filter, we assume that the two rings resonate at $\lambda_{\mathrm{MR\_0}}$ and $\lambda_{\mathrm{MR\_0}} + 2\delta$, respectively, with a 2δ deviation in resonant wavelength. The two rings have the same 3-dB bandwidth of 2δ. The spectral response of the two-ring parallel-coupled add-drop filter is shown in Fig. 6, if the phase delay between the two rings satisfies the condition that $\theta = 2\pi N + \pi/2$. The spectral response has double peaks, and the 3-dB bandwidth is nearly two times wider as compared to the Lorentzian power transfer of a single ring. At the two peaks, nearly full power transfer is achieved ($\kappa_p^2/\kappa^2 \ll 1$). At the middle of the passband, the total power transmission is found to be about 0.89.

For a four-ring parallel-coupled add-drop filter, we assume that the rings resonate respectively at $\lambda_{\mathrm{MR\_0}}$, $\lambda_{\mathrm{MR\_0}} + 2\delta$,

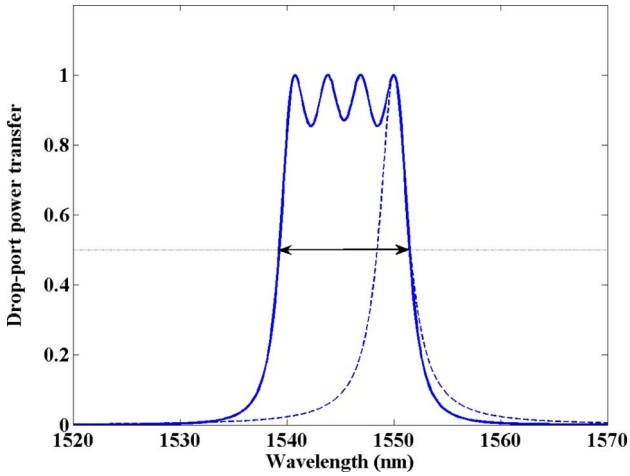

Fig. 7. Drop-port power transfer function of the four-ring parallel-coupled add-drop filter, assuming $\theta = 2\pi N + \pi/2$ and $\kappa_p^2/\kappa^2 \ll 1$.

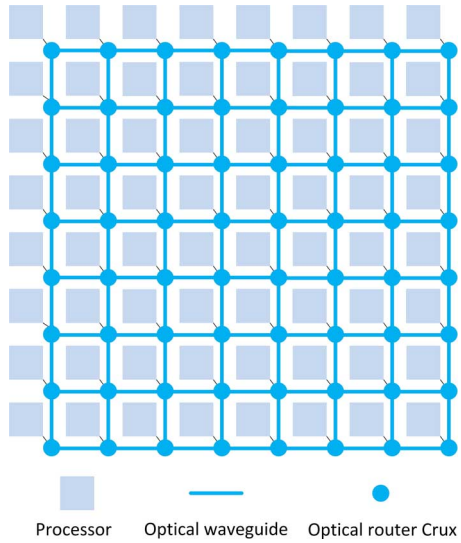

Fig. 8. 8 × 8 mesh-based optical NoC.

$\lambda_{\mathrm{MR\_0}}+4\delta$, and $\lambda_{\mathrm{MR\_0}}+6\delta$, with a 2δ wavelength deviation between each two neighboring rings. The four rings have the same 3-dB bandwidth of 2δ. If the phase delay between each two neighboring rings satisfies the condition that $\theta = 2\pi N + \pi/2$, the overall power transfer from the input port to the drop port in the four-ring parallel-coupled add-drop filter is shown in Fig. 7. Nearly full power transfer is achieved at the four peaks while assuming $\kappa_p^2/\kappa^2 \ll 1$, and the 3-dB bandwidth is about four times wider as compared to the single-ring add-drop filter. At the center of the passband, the overall power transmission in the drop port is found to be about 0.87. As shown above, the 3-dB bandwidth of add-drop filters is expected to expand nearly linearly by periodically coupling multiple rings. This feature of high-order parallel-coupled add-drop filters should be useful to provide better thermal tolerance for ONoCs. But considering the higher cost of high-order add-drop filters, designers should make tradeoff decisions.

D. Minimize the Number of Switching Stages in ONoC Architectures

The number of switching stages N in an optical link directly affects the optical power loss on the path. For mesh-based ONoCs (see Fig. 8) with XY routing (2-D order routing), we can use a passive-routing optical router Crux (see Fig. 9) to minimize the number of switching stages. Crux is a compact low-loss 5 × 5 strictly non-blocking optical switching fabric [51]. It does not need to turn on any microresonator if an optical signal travels in the same direction through the router, such as from north to south or from west to east. And only one microresonator will be powered on if an optical signal makes a turn or uses the injection/ejection port. Because of the passive routing feature of Crux, the maximum number of switching stages in a XY-routing optical mesh is three, regardless of the network size.

E. Evaluation and Comparison of Worst-Case Power Consumption of OnoC

In this section, we compared the worst-case power consumption of ONoCs with different techniques proposed. The worst-case analysis is conducted among all possible thermal maps where the chip temperature varying spatially between 55 °C and 85 °C.

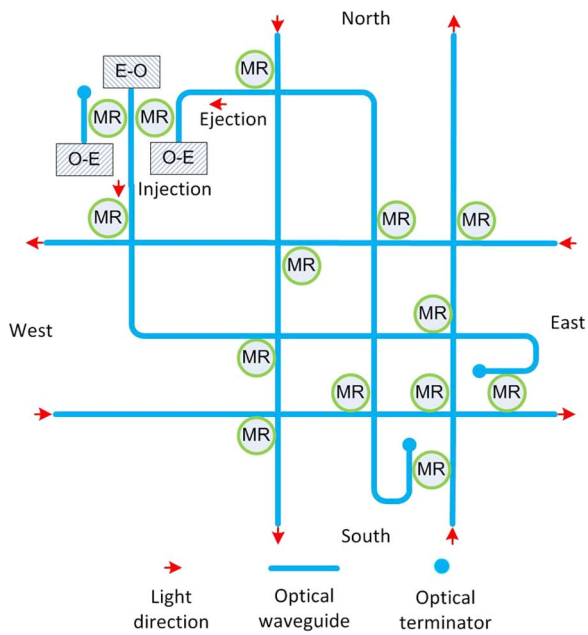

Fig. 9. Optical router Crux.

Fig. 10 shows the worst-case power consumption of an optical link with three switching stages. We assume that the 3-dB bandwidth of a single microresonator is 1.55 nm and we double the 3-dB bandwidth to 3.1 nm by replacing each microresonator with a two-ring parallel-coupled add-drop filter. In an 8 × 8 mesh-based optical NoC built by Crux, after we replace each microresonator with two parallel-coupling rings, there would be 1792 microresonators. Assume that every microresonator is of 5 μm radius [39], the total area of microresonators is about 0.15 mm^2. The total area of microresonators would increase to 0.3 mm^2 if we use the four-ring design rather than two-ring parallel-coupled filters. We consider the fabrication variation of microresonators and assume that the actual resonant wavelength

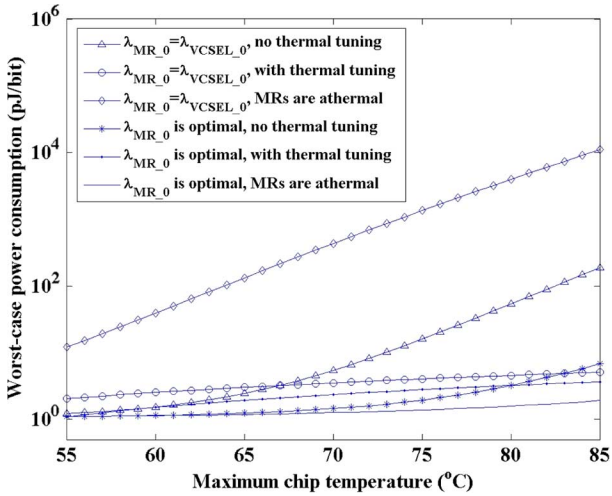

Fig. 10. Worst-case power consumption under different configurations.

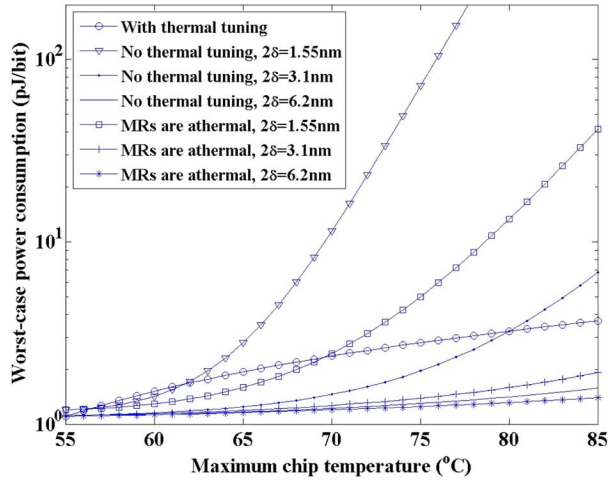

Fig. 11. Worst-case power consumption with different 3-dB bandwidths.

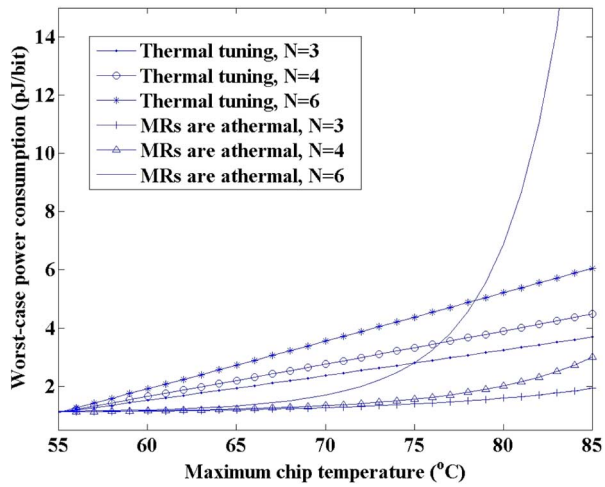

Fig. 12. Worst-case power consumption under different numbers of switching stage in a link.

after fabrication is a Gaussian distribution with a standard deviation of 0.4 nm [43]. Fig. 10 shows that with the default initial setting of $\lambda_{\mathrm{MR\_0}} = \lambda_{\mathrm{VCSEL\_0}}$, the worst-case power efficiency will drop to about 180 pJ/bit. By applying local thermal tuning of microresonators with microheaters to compensate the wavelength shift caused by temperature variation as well as fabrication variation, the worst-case power consumption can be improved to 5.2 J/bit. The optimal setting of $\lambda_{\mathrm{MR\_0}}$ can further reduce the worst-case thermal-induced power loss and improve the power efficiency by 29% to 3.7 pJ/bit.

One observation from Fig. 10 is that, when using on-chip VCSELs as laser sources, the use of athermal microresonators with $\lambda_{\mathrm{MR\_0}} = \lambda_{\mathrm{VCSEL\_0}}$ does not help but even makes the power efficiency worse. Though athermal microresonators do not have temperature dependence, wavelength mismatch still exists in switching because of the VCSEL lasing variation under temperature fluctuations. The resonance wavelength of athermal microresonators should also be set according to the optimal condition in (21). In this case, the worst-case power consumption can be reduced to 1.9 pJ/bit, which is even more efficient than using thermal tuning to compensate wavelength mismatches.

All these evaluations assume that the 3-dB bandwidth has been increased from 1.55 to 3.1 nm by the proposed parallel-coupling rings. Fig. 11 shows the worst-case power consumption of ONoCs with different 3-dB bandwidths. The number of switching stages is three and we assume that microresonators resonant wavelength are set according to the optimal condition. For ONoCs with thermal tuning, since we assume that microresonators are always tuned to match the signal wavelength, the 3-dB bandwidth would not affect the power consumption and the worst-case power efficiency is 3.7 pJ/bit. If the 3-dB bandwidth is 1.55 nm, the worst-case power consumption with athermal microresonators is as high as 41 pJ/bit. If we increase the 3-dB bandwidth from 3.1 to 6.2 nm, the worst-case power efficiency with athermal microresonators would improve from 1.9 to 1.4 pJ/bit. Even if the microresonators are temperature sensitive, when the 3-dB bandwidth is wide, e.g., 6.2 nm, the worst-case power efficiency without thermal tuning can be lowered to 1.6 pJ/bit. These results show that on the basis of optimal initial device setting, the power efficiency of ONoCs with athermal microresonators could be better than with thermal tuning if the 3-dB bandwidth is wide. But thermal tuning would outperform in worst-case power consumption if the 3-dB bandwidth is not wide enough.

Fig. 12 shows the worst-case power consumption of ONOCs with different number of switching stages. We assume the initial setting of microresonator resonant wavelength is optimal, and the microresonator 3-dB bandwidth is 3.1 nm. By using thermal tuning for temperature compensation, the worst-case power consumption increases to 4.5 and 6 pJ/bit respectively when $N = 4$ and $N = 6$. On the other hand, if the microresonators are designed to be athermal, the worst-case power consumption increases dramatically to 24 pJ/bit when the number of switching stages is six. It can be concluded that for ONoCs using either thermal tuning or athermal microresonators, besides setting the device parameters according to (21), it is also important to keep the number of switching stages as small as possible. The use of passive-routing optical router like Crux (see Fig. 9) is an effective way to minimize the number of switching stages in mesh-based ONoCs.

V. Analysis of Thermal Effects in a Mesh-Based Optical NoC under MPSoC Applications

In previous section, we conducted the worst-case analysis for packet transmissions in all possible links of an ONoC. In this section, we used an 8 × 8 mesh-based ONoC (see Fig. 8) as a case study and evaluated its power consumption under different MPSoC applications. We also quantitatively analyzed the impacts of thermal effects in the average power efficiency. This paper provided a general model to study the thermal effects in ONoCs. And the analysis of other ONoC architectures would be similar. The set of real MPSoC applications include FPPPP (SPEC fpppp), H264DH (H.264 decoder with high resolution), SAMPLE (sample rate converter), and SATELL (satellite receiver). For each application, an offline optimization approach was applied for task mapping and scheduling onto the 8 × 8 optical mesh NoC-based MPSoC [52]. It uses formal computational models to capture both communication and computation requirements for each application, and maximizes the overall system performance and utilization. This realistic traffic benchmark suite enables a better study of NoC characteristics than using traditional random traffic patterns.

The 8 × 8 mesh-based ONoC is a circuit-switched network with an electronic control network for path maintenance. Before each packet transmission, an optical path is reserved and configured by routing setup packet in the electronic control network. XY routing is used for path selection. Each packet is routed first in X dimension until it reaches the node in the same column with the destination, and then along the perpendicular Y dimension to the destination. It is a low-complexity distributed algorithm without any routing table, and destination address is the only information required to find the next hop. Payload data is transmitted along the reserved optical path after path setup. High-speed optical transmission is achieved without buffering in intermediate routers. After finishing payload transmission, the optical path would be released by routing a tear-down packet along the reserved path in the electronic control network.

The power consumption for a packet transmission involves the energy consumed for payload transmission in optical domain and the energy consumed for routing control packets in electronic domain. The energy consumption for a control packet is estimated as the energy required to transfer it through all the electrical interconnects, electronic switching fabrics, and control units along the path in the electronic control network. The energy consumed by a payload transmission includes the energy consumed by O/E interfaces, and microresonator energy consumption in the optical path. Since the size of control packets is small, the power consumed in the electronic control network only takes a small proportion, and the power consumption in O/E interfaces accounts for the major proportion of the total energy consumption. A typical O/E interface includes serializer/deserializer, laser driver, VCSEL, optical waveguide, photodetector, and TIA-LA circuits. For evaluation of power consumption for O/E conversions, we use the serializer and deserializer designs in [53], and the VCSEL driver and TIA-LA circuit designs in [54]. The power consumption for turning on a microresonator is assumed to be 20 μW.

Based on the thermal model, we evaluated the communication power consumption of the Crux-based 8 × 8 optical mesh NoC for running one application iteration under different MPSoC applications. By using Crux as the optical routers, the number of switching stages in the mesh-based optical NoC is minimized. As for 3-dB bandwidth, we assume that the 3-dB bandwidth of a single microresonator is 1.55 nm, and we double the 3-dB bandwidth to 3.1 nm by replacing each microresonator with two parallel-coupling rings. Fig. 13 shows the evaluation results of communication power consumption for running applications with different proposed techniques including optimal initial device settings, thermal tuning and athermal microresonators. We assume the chip temperature varies spatially between 55 °C and 85 °C. We consider the resonant wavelength after fabrication as a Gaussian distribution with a standard deviation of 0.4 nm [43]. For the application of SPEC fpppp, the communication power consumption for one application iteration is about 8.86 μJ if the initial microresonator resonance wavelength $\lambda_{\mathrm{MR\_0}}$ is set to equal to $\lambda_{\mathrm{VCSEL\_0}}$. By using thermal tuning to compensate microresonator wavelength shift caused by temperature variation as well as fabrication variation, the power consumption is improved to 4.47 μJ. By setting microresonator resonance wavelength according to the optimal condition, the communication power consumption for one application iteration can be further reduced by half to 2.04 μJ. Evaluation results for other three applications show a similar trend that, the best combination of proposed techniques improves the power efficiency by more than 70%.

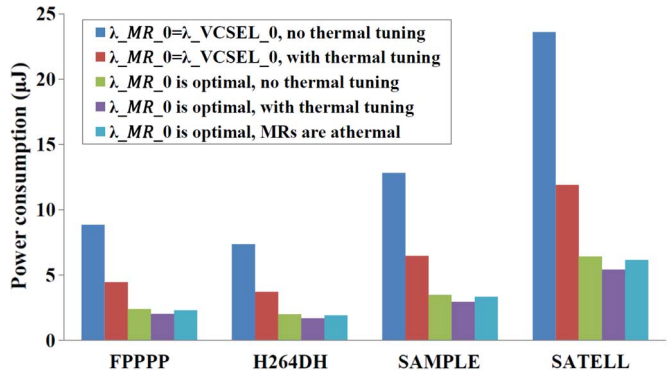

Fig. 13. Power consumption of a Crux-based optical mesh under different MPSoC applications, the maximum chip temperature $T_{\max} = 85\,^{\circ}\mathrm{C}$.

Fig. 14 shows the average power efficiency of the Crux-based optical mesh under different maximum chip temperatures. We assume that two-ring parallel-coupled add-drop filters are used and the 3-dB bandwidth is 3.1 nm. If the initial microresonator resonance wavelength $\lambda_{\mathrm{MR\_0}}$ is equal to $\lambda_{\mathrm{VCSEL\_0}}$, the average communication power efficiency for the four real MPSoC applications is 5.2 pJ/bit when the maximum chip temperature reaches 85 °C. It can be improved to about 2.6 pJ/bit if thermal tuning is applied. By setting the optimal initial device conditions, the average power efficiency is further improved by 54% to about 1.2 pJ/bit. If the microresonators are athermal and their resonance wavelength are set to the optimal, the average power efficiency of the optical mesh is about 1.34 pJ/bit. By combing the technique of optimal device setting with thermal tuning or the technique of temperature-insensitive microresonators, good

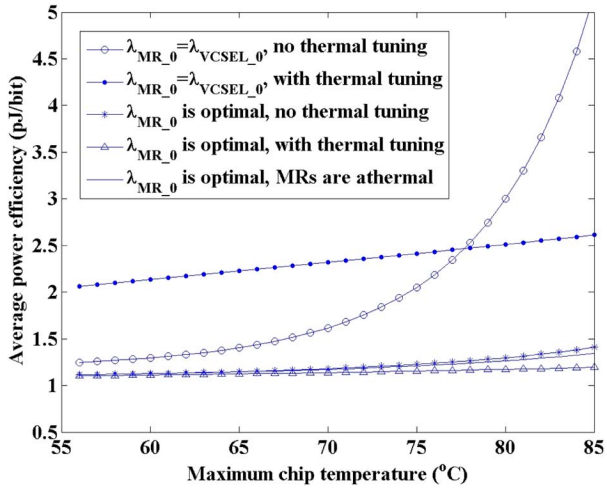

Fig. 14. Average power efficiency of a Crux-based optical mesh with different configurations.

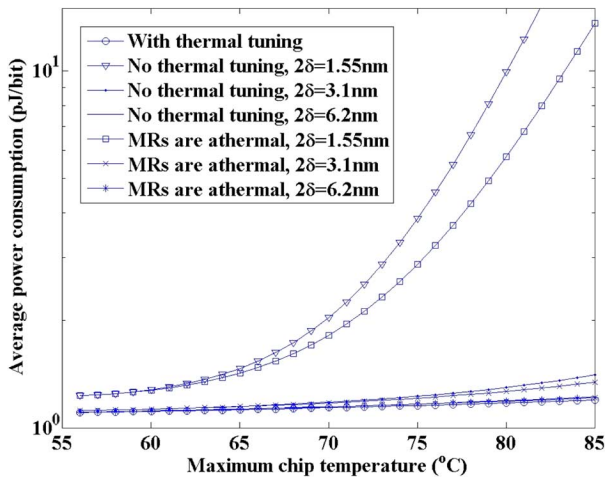

Fig. 15. Average power efficiency of a Crux-based optical mesh with different 3-dB bandwidths.

power efficiency can be achieved even under large on-chip temperature fluctuations. Since thermal tuning and athermal microresonators cause additional costs such as the implementation of local microheaters and higher fabrication cost, designers should make tradeoff decisions.

All these evaluations assume that the 3-dB bandwidth has been increased from 1.55 to 3.1 nm by the proposed parallel-coupled rings. Fig. 15 shows the comparison of average power consumption with different 3-dB bandwidths. We assume that microresonators resonant wavelengths are set according to the optimal condition. For ONoCs with thermal tuning, since we assume that microresonators are always tuned to match the signal wavelength, the 3-dB bandwidth would not affect the power consumption and the average power efficiency is 1.2 pJ/bit. If the 3-dB bandwidth is 1.55 nm, the average power consumption with athermal microresonators is 13.5 pJ/bit. If we increase the 3-dB bandwidth from 3.1 to 6.2 nm, the average power efficiency would be improved from 1.34 to 1.21 pJ/bit. And even if the microresonators are temperature sensitive, when the 3-dB bandwidth is wide enough, e.g., 6.2 nm, the average power efficiency without thermal tuning can be lowered to 1.23 pJ/bit. These results show that on the basis of optimal initial device setting, thermal tuning would outperform the use of athermal microresonators if the 3-dB bandwidth is not wide. If the 3-dB bandwidth is wide, e.g., 3.1 nm, the average power efficiency of ONoCs with athermal microresonators would become much closer to those with thermal tuning.

VI. Conclusion

We systematically analyzed the temperature sensitivity of ONoCs, and developed an analytical ONoC thermal model. We revealed three important factors regarding ONoC power efficiency under temperature variations, including the initial setting of photonic devices, the number of switching stages in the ONoC architecture, and the bandwidth of optical switching elements. We used an 8×8 mesh-based ONoC as a case study and quantitatively evaluated its temperature-dependent average power efficiency under real MPSoC applications. A passive-routing optical router Crux was used in the optical mesh to minimize the number of switching stages in XY routing. We found the optimal setting of initial resonance for microresonators, and took advantage of parallel coupling of multiple microresonators to increase the 3-dB bandwidth. A mathematical analysis of periodical parallel coupling was given in this work, and we show that the 3-dB bandwidth of the spectral power response can be widened nearly linearly with the ring number. By combing the technique of optimal device setting with other related techniques such as thermal tuning or temperature-insensitive microresonators, good power efficiency can be achieved even under large on-chip temperature fluctuations. For the 8×8 mesh-based ONoC under real MPSoC applications, on the basis of thermal tuning, the optimal setting of microresonator resonance improves the average power efficiency by 54% to 1.2 pJ/bit when the maximum chip temperature reaches 85 °C.

References

[1] W. Dally and B. Towles, "Route packets, not wires: On-chip interconnection networks," in *Proc. Design Autom. Conf.*, 2001, pp. 684–689.

[2] L. Benini and G. De Micheli, "Networks on chip: A new paradigm for systems on chip design," in *Proc. Design, Autom., Test Euro. Conf. Exhib.*, 2002, pp. 418–419.

[3] I. Young, E. Mohammed, J. Liao, A. Kern, S. Palermo, B. Block, M. Reshotko, and P. Chang, "Optical I/O technology for tera-scale computing," in *Proc. IEEE Int. Solid-State Circuits Conf.*, 2009, pp. 468–469.

[4] K. Skadron, M. R. Stan, K. Sankaranarayanan, W. Huang, S. Velusamy, and D. Tarjan, "Temperature-aware microarchitecture: Modeling and implementation," *ACM Trans. Arch. Code Optim.*, vol. 1, no. 1, pp. 94–125, 2004.

[5] Y. Ye, J. Xu, X. Wu, W. Zhang, X. Wang, M. Nikdast, Z. Wang, and W. Liu, "Modeling and analysis of thermal effects optical networks-on-chip," in *Proc. IEEE Comput. Soc. Annu. Symp. VLSI*, 2011, pp. 254–259.

[6] N. Kirman, M. Kirman, R. Dokania, J. Martinez, A. Apsel, M. Watkins, and D. Albonesi, "On-chip optical technology future bus-based multi-core designs," *IEEE Micro*, vol. 27, no. 1, pp. 56–66, Jan./Feb. 2007.

[7] M. Briere, B. Girodias, Y. Bouchebaba, G. Nicolescu, F. Mieyeville, F. Gaffiot, and I. O'Connor, "System level assessment of an optical NoC an MPSoC platform," in *Design, Autom., Test Euro. Conf. Exhib.*, 2007, pp. 1–6.

[8] R. Beausoleil, J. Ahn, N. Binkert, A. Davis, D. Fattal, M. Fiorentino, N. Jouppi, M. McLaren, C. Santori, R. Schreiber, S. Spillane, D. Vantrease, and Q. Xu, "A nanophotonic interconnect for high-performance many-core computation," in *Proc. IEEE Symp. High Perform. Interconnects*, 2008, pp. 182–189.

[9] A. Shacham, K. Bergman, and L. Carloni, "On the design of a photonic network-on-chip," in *Proc. Int. Symp. Netw.-on-Chip*, 2007, pp. 53–64.

[10] K. H. Mo, Y. Ye, X. Wu, W. Zhang, W. Liu, and J. Xu, "A hierarchical hybrid optical-electronic network-on-chip," in *Proc. IEEE Comput. Soc. Annu. Symp. VLSI*, 2010, pp. 327–332.

[11] S. Pasricha and N. Dutt, "Orb: An on-chip optical ring bus communication architecture for multi-processor systems-on-chip," in *Proc. Asia South Pacific Conf. Design Autom.*, 2008, pp. 789–794.

[12] Y. Pan, P. Kumar, J. Kim, G. Memik, Y. Zhang, and A. Choudhary, "Firefly: Illuminating future network-on-chip with nanophotonics," in *Proc. Int. Symp. Comput. Arch. (ISCA)*, 2009, pp. 429–440.

[13] H. Gu, J. Xu, and W. Zhang, "A low-power fat tree-based optical network-on-chip for multiprocessor system-on-chip," in *Proc. Design, Autom. Test Euro. Conf. Exhib.*, 2009, pp. 3–8.

[14] M. J. Cianchetti, J. C. Kerekes, and D. H. Albonesi, "Phastlane: A rapid transit optical routing network," in *Proc. Annu. Int. Symp. Comput. Arch. ACM*, 2009, pp. 441–450.

[15] A. Kodi, R. Morris, A. Louri, and X. Zhang, "On-chip photonic interconnects for scalable multi-core architectures," in *Proc. ACM/IEEE Int. Symp. Netw.-on-Chip*, 2009, p. 90.

[16] D. Ding, Y. Zhang, H. Huang, R. Chen, and D. Pan, "O-router: An optical routing framework for low power on-chip silicon nano-photonic integration," in *Proc. ACM/IEEE Design Autom. Conf.*, 2009, pp. 264–269.

[17] C. Batten, A. Joshi, J. Orcutt, A. Khilo, B. Moss, C. Holzwarth, M. Popovic, H. Li, H. Smith, J. Hoyt, F. Kartner, R. Ram, V. Stojanovic, and K. Asanovic, "Building manycore processor-to-dram networks with monolithic silicon photonics," in *Proc. IEEE Symp. High Perform. Interconnects*, 2008, pp. 21–30, 26–28.

[18] R. K. Dokania and A. B. Apsel, "Analysis of challenges for on-chip optical interconnects," in *Proc. ACM Great Lakes Symp. VLSI*, 2009, pp. 275–280.

[19] Z. Li, M. Mohamed, X. Chen, E. Dudley, K. Meng, L. Shang, A. R. Mickelson, R. Joseph, M. Vachharajani, B. Schwartz, and Y. Sun, "Reliability modeling and management of nanophotonic on-chip networks," *IEEE Trans. Very Large Scale Integr. (VLSI) Syst.*, vol. 20, no. 1, pp. 98–111, Jan. 2012.

[20] T. Baehr-Jones, M. Hochberg, C. Walker, E. Chan, D. Koshinz, W. Krug, and A. Scherer, "Analysis of the tuning sensitivity of silicon-on-insulator optical ring resonators," *J. Lightw. Technol.*, vol. 23, no. 12, pp. 4215–4221, Dec. 2005.

[21] V. Padgaonkar and A. Arbor, "Thermal effects silicon based resonant cavity devices," NNIN REU Research Accomplishments, 2004.

[22] P. Dumon, G. Priem, L. Nunes, W. Bogaerts, D. Van Thourhout, P. Bienstman, T. Liang, M. Tsuchiya, P. Jaenen, S. Beckx, J. Wouters, and R. Baets, "Linear and nonlinear nanophotonic devices based on silicon-on-insulator wire waveguides," *Japan. J. Appl. Phys.*, vol. 45, pp. 6589–6602, 2006.

[23] F. Gan, T. Barwicz, M. Popovic, M. Dahlem, C. Holzwarth, P. Rakich, H. Smith, E. Ippen, and F. Kartner, "Maximizing the thermo-optic tuning range of silicon photonic structures," *Photon. Switching*, pp. 67–68, Aug. 2007.

[24] M. Geng, L. Jia, L. Zhang, L. Yang, P. Chen, T. Wang, and Y. Liu, "Four-channel reconfigurable optical add-drop multiplexer based on photonic wire waveguide," *Opt. Expr.*, vol. 17, no. 7, pp. 5502–5516, Mar. 2009.

[25] J.-M. Lee, D.-J. Kim, H. Ahn, S.-H. Park, and G. Kim, "Temperature dependence of silicon nanophotonic ring resonator with a polymeric overlayer," *J. Lightw. Technol.*, vol. 25, no. 8, pp. 2236–2243, Aug. 2007.

[26] V. Raghunathan, J. Hu, W. N. Ye, J. Michel, and L. C. Kimerling, "Athermal silicon ring resonators," *Integr. Photon. Res., Silicon, Nanophoton.*, p. IMC5, 2010.

[27] R. Michalzik and K. J. Ebeling, "Operating principles of VCSELs," Optoelectron. Dept., Univ. Ulm, Ulm, Germany, 2003.

[28] S. Mogg, N. Chitica, U. Christiansson, R. Schatz, P. Sundgren, C. Asplund, and M. Hammar, "Temperature sensitivity of the threshold current of long-wavelength InGaAs-GaAs VCSELs with large gain-cavity detuning," *IEEE J. Quantum Electron.*, vol. 40, no. 5, pp. 453–462, May. 2004.

[29] A. Syrbu, A. Mereuta, V. Iakovlev, A. Caliman, P. Royo, and E. Kapon, "10 Gbps VCSELs with high single mode output 1310 nm and 1550 nm wavelength bands," in *Proc. Conf. Opt. Fiber Commun./Nat. Fiber Opt. Eng.*, 2008, pp. 1–3.

[30] S. Koester, L. Schares, C. Schow, G. Dehlinger, and R. John, "Temperature-dependent analysis of Ge-on-SOI photodetectors and receivers," in *Proc. IEEE Int. Conf. Group IV Photon.*, 2006, pp. 179–181.

[31] M. Morse, O. Dosunmu, G. Sarid, and Y. Chetrit, "Performance of Ge-on-Si p-i-n photodetectors for standard receiver modules," *IEEE Photon. Technol. Lett.*, vol. 18, no. 23, pp. 2442–2444, Dec. 2006.

[32] D. Li, S.-D. Tan, E. Pacheco, and M. Tirumala, "Architecture-level thermal characterization for multicore microprocessors," *IEEE Trans. Very Large Scale Integr. (VLSI) Syst.*, vol. 17, no. 10, pp. 1495–1507, Oct. 2009.

[33] W. Huang, "Hotspot: A chip and package compact thermal modeling methodology for VLSI design," Ph.D. dissertation, Dept. Elect. Comput. Eng., Univ. Virginia, Blacksburg, 2007.

[34] M. Iyengar and R. Schmidt, "Analytical modeling for prediction of hot spot chip junction temperature for electronics cooling applications," in *Proc. Intersociety Conf. Thermal Thermomech. Phenomena Electron. Syst.*, 2006, pp. 87–95.

[35] F. G. Della Corte, M. Esposito Montefusco, L. Moretti, I. Rendina, and G. Cocorullo, "Temperature dependence analysis of the thermo-optic effect silicon by single and double oscillator models," *J. Appl. Phys.*, vol. 88, no. 12, pp. 7115–7119, Dec. 2000.

[36] J. M. Perkins, T. L. Simpkins, C. Warde, and J. Clifton G. Fonstad, "Full recess integration of small diameter low threshold VCSELs with si-cmos ics," *Opt. Expr.*, vol. 16, no. 18, pp. 13, 955–13, 960, Sep. 2008.

[37] C. Chen, P. Leisher, A. Allerman, K. Geib, and K. Choquette, "Temperature analysis of threshold current infrared vertical-cavity surface-emitting lasers," *IEEE J. Quantum Electron.*, vol. 42, no. 10, pp. 1078–1083, Oct. 2006.

[38] R. Amatya, C. Holzwarth, M. Popovic, F. Gan, H. Smith, F. Kartner, and R. Ram, "Low power thermal tuning of second-order microring resonators," in *Proc. Conf. Lasers Electro-Opt.*, 2007, pp. 1–2.

[39] S. Xiao, M. H. Khan, H. Shen, and M. Qi, "Compact silicon microring resonators with ultra-low propagation loss the C band," *Opt. Expr.*, vol. 15, no. 22, pp. 14 467–14 475, 2007.

[40] B. G. Lee, B. A. Small, K. Bergman, Q. Xu, and M. Lipson, "Transmission of high-data-rate optical signals through a micrometer-scale silicon ring resonator," *Opt. Lett.*, vol. 31, no. 18, pp. 2701–2703, 2006.

[41] S. Xiao, M. H. Khan, H. Shen, and M. Qi, "Modeling and measurement of losses silicon-on-insulator resonators and bends," *Opt. Expr.*, vol. 15, no. 17, pp. 10 553–10 561, 2007.

[42] S. Xiao, M. H. Khan, H. Shen, and M. Qi, "Multiple-channel silicon micro-resonator based filters for WDM applications," *Opt. Expr.*, vol. 15, no. 12, pp. 7489–7498, 2007.

[43] F. A. Xia, L. A. Sekaric, and Y. T. Vlasov, "Ultracompact optical buffers on a silicon chip," *Nature Photon.*, no. 1, pp. 65–71, 2007.

[44] Y. Vlasov and S. McNab, "Losses single-mode silicon-on-insulator strip waveguides and bends," *Opt. Expr.*, vol. 12, no. 8, pp. 1622–1631, 2004.

[45] E. Margallo-Balbás, M. Geljon, G. Pandraud, and P. J. French, "Miniature 10 kHz thermo-optic delay line silicon," *Opt. Lett.*, vol. 35, no. 23, pp. 4027–4029, Dec. 2010.

[46] G. Masini, G. Capellini, J. Witzens, and C. Gunn, "A 1550 nm, 10 Gbps monolithic optical receiver 130 nm CMOS with integrated Ge waveguide photodetector," in *Proc. IEEE Int. Conf. Group IV Photon.*, 2007, pp. 1–3.

[47] X. Zheng, F. Liu, D. Patil, H. Thacker, Y. Luo, T. Pinguet, A. Mekis, J. Yao, G. Li, J. Shi, K. Raj, J. Lexau, E. Alon, R. Ho, J. E. Cunningham, and A. V. Krishnamoorthy, "A sub-picojoule-per-bit CMOS photonic receiver for densely integrated systems," *Opt. Expr.*, vol. 18, no. 1, pp. 204–211, Jan. 2010.

[48] B. Little, S. Chu, H. Haus, J. Foresi, and J.-P. Laine, "Microring resonator channel dropping filters," *J. Lightw. Technol.*, vol. 15, no. 6, pp. 998–1005, Jun. 1997.

[49] B. E. Little, S. T. Chu, J. V. Hryniewicz, and P. P. Absil, "Filter synthesis for periodically coupled microring resonators," *Opt. Lett.*, vol. 25, no. 5, pp. 344–346, 2000.

[50] M.-C. M. Lee and M. C. Wu, "Variable bandwidth of dynamic add-drop filters based on coupling-controlled microdisk resonators," *Opt. Lett.*, vol. 31, no. 16, pp. 2444–2446, 2006.

[51] Y. Xie, M. Nikdast, J. Xu, W. Zhang, Q. Li, X. Wu, Y. Ye, X. Wang, and W. Liu, "Crosstalk noise and bit error rate analysis for optical network-on-chip," in *Proc. ACM/IEEE Design Autom. Conf.*, 2010, pp. 657–660.

[52] W. Liu, J. Xu, X. Wu, Y. Ye, X. Wang, W. Zhang, M. Nikdast, and Z. Wang, "A NoC traffic suite based on real applications," in *Proc. IEEE Comput. Soc. Annu. Symp. VLSI*, 2011, pp. 66–71.

[53] J. Poulton, R. Palmer, A. Fuller, T. Greer, J. Eyles, W. Dally, and M. Horowitz, "A 14-mW 6.25-Gb/s transceiver 90-nm CMOS," *IEEE J. Solid-State Circuits*, vol. 42, no. 12, pp. 2745–2757, Dec. 2007.

[54] C. Kromer, G. Sialm, C. Berger, T. Morf, M. Schmatz, F. Ellinger, D. Erni, G.-L. Bona, and H. Jackel, "A 100-mW 4 × 10 Gb/s transceiver 80-nm CMOS for high-density optical interconnects," *IEEE J. Solid-State Circuits*, vol. 40, no. 12, pp. 2667–2679, Dec. 2005.

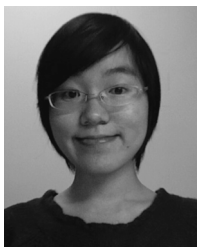

Yaoyao Ye (S'09) received the B.S. degree in electronic engineering from University of Science and Technology of China, Hefei, China, in 2008. She is currently pursuing the Ph.D. degree in electronic and computer engineering from Hong Kong University of Science and Technology, Hong Kong.

Her research interests include network-on-chip, multiprocessor system-on-chip, and embedded system.

Jiang Xu (S'02–M'07) received the Ph.D. degree from Princeton University, Princeton, NJ, in 2007.

From 2001 to 2002, he was a Research Associate with Bell Labs, NJ. He was a Research Associate with NEC Laboratories America, NJ, from 2003 to 2005. He joined a startup company, Sandbridge Technologies, NY, from 2005 to 2007 and developed as well as implemented two generations of NoC-based ultra-low power multiprocessor systems-on-chip for mobile platforms. In 2007, he joined the Department of Electronic and Computer Engineering, Hong Kong University of Science and Technology, as an Assistant Professor, and established the Mobile Computing System Lab. He authored or coauthored over 50 book chapters and papers in peer-reviewed journals and international conferences. His research areas include network-on-chip, multiprocessor system-on-chip, embedded system, computer architecture, low-power VLSI design, and HW/SW codesign.

Dr. Xu currently serves as an Associate Editor of *ACM Transactions on Embedded Computing Systems* and IEEE TRANSACTIONS ON VERY LARGE SCALE INTEGRATION (VLSI) SYSTEMS. He is an ACM Distinguished Speaker and a Distinguished Visitor of IEEE Computer Society. He served on the organizing committees and technical program committees of many international conferences.

Xiaowen Wu (S'12) received B.Sc. degree in computer science from the Harbin Institute of Technology, Harbin, China, in 2008. He is currently pursuing the Ph.D. degree in electronic and computer engineering from the Hong Kong University of Science and Technology, Hong Kong.

His research interests include embedded systems, multiprocessor systems, and network-on-chip.

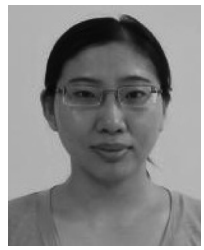

Wei Zhang (M'05) received the Bachelor's and Master's degrees in electrical engineering from Harbin Institute of Technology, Harbin, China, in 1999 and 2001, respectively, and the Ph.D degree in computer engineering from Princeton University, Princeton, NJ, in 2009.

She is currently an Assistant Professor with the School of Computer Engineering, Nanyang Technological University, Singapore.

Dr. Zhang was a recipient of a Princeton Research Prize and a Best Paper Award in 2007 and 2009, respectively. Her research interests include embedded systems, reconfigurable computing, nanotechnology, electronic design automation, and network-on-chip. She is a member of the ACM.

Xuan Wang (S'12) received the B.S. degree in electrical engineering from Shanghai Jiaotong University, Shanghai, China, in 2009. He is currently pursuing the Ph.D. degree in electronic and computer engineering from Hong Kong University of Science and Technology (HKUST), Hong Kong.

His research interests include embedded system, multiprocessor system, network-on-chip and fault tolerant design and reliability issues in very deep submicrometer technologies.

Mahdi Nikdast (S'10) received the B.Sc. degree in computer engineering (with honors) from Islamic Azad University, Esfahan, Iran, in 2009. He is currently pursuing the Ph.D. degree from the Mobile Computing System Laboratory, Hong Kong University of Science and Technology, Hong Kong, where he is currently focusing on SNR analyses for ONoCs.

His research interests include embedded systems, multiprocessor systems-on-chip, networks-on-chip, and computer architecture.

Zhehui Wang (S'12) received the B.S. degree in electrical engineering from Fudan University, Fudan, China, in 2010. He is currently pursuing the Ph.D. degree from the Department of Electronic and Computer Engineering, Hong Kong University of Science and Technology, Hong Kong.

His research interests include embedded system, multiprocessor systems, network-on-chip, and floorplan design for network-on-chip.

Weichen Liu (S'07–M'11) received the B.S. and M.S. degrees from Harbin Institute of Technology, Harbin, China, in 2004 and 2006, and the Ph.D. degree from the Hong Kong University of Science and Technology, Hong Kong, in 2011, all in computer science and engineering.

His research interests include real-time embedded systems, multiprocessor systems and network-on-chip.